

# Artificial Neural Network Based Computation for Out-of-Time-Ordered Correlators

Yukai Wu,<sup>1</sup> L.-M. Duan,<sup>1,\*</sup> and Dong-Ling Deng<sup>1,†</sup>

<sup>1</sup>Center for Quantum Information, IIIS, Tsinghua University, Beijing 100084, P. R. China

(Dated: December 11, 2019)

Out-of-time-ordered correlators (OTOCs) are of crucial importance for studying a wide variety of fundamental phenomena in quantum physics, ranging from information scrambling to quantum chaos and many-body localization. However, apart from a few special cases, they are notoriously difficult to compute even numerically due to the exponential complexity of generic quantum many-body systems. In this paper, we introduce a machine learning approach to OTOCs based on the restricted-Boltzmann-machine architecture, which features wide applicability and could work for arbitrary-dimensional systems with massive entanglement. We show, through a concrete example involving a two-dimensional transverse field Ising model, that our method is capable of computing early-time OTOCs with respect to random pure quantum states or infinite-temperature thermal ensembles. Our results showcase the great potential for machine learning techniques in computing OTOCs, which open up numerous directions for future studies related to similar physical quantities.

Out-of-time-ordered correlators (OTOCs), first introduced by Larkin and Ovchinnikov in the context of superconductivity [1], have attracted tremendous attention across different communities, including quantum information, high-energy physics, and condensed matter physics. Through analytical and numerical studies, OTOCs of various many-body quantum systems have been computed to characterize their properties in quantum information scrambling [2–12], quantum chaos [2, 13–15] and equilibrium and dynamical quantum phase transitions [16–18]. In addition, it has been shown that OTOCs would shed new light on the study of quantum gravity and black holes via AdS/CFT duality [19–27]. Recently, OTOCs have also been experimentally measured in systems of trapped ions [28], solid-state spins [29, 30], and <sup>87</sup>Rb Bose-Einstein condensate [31], etc. Here, we introduce machine learning, an important tool borrowed from computer science [32–34], to the studies of OTOCs, with focus on numerical computation of OTOCs by using restricted Boltzmann machines (RBMs) (see Fig. 1 for a schematic illustration).

Apart from some analytically solvable examples (e.g. [35–39]), the numerical computation of OTOCs for generic quantum many-body systems is notoriously challenging due to the exponential scaling of the Hilbert space dimension with the system size. In one-dimensional (1D) systems with short-range interaction, OTOCs can be computed using tensor network methods such as time evolving block decimation (TEBD) [16] and matrix product operators (MPO) [40]. However, once long-range interactions are included, these methods may no longer be efficient since the entanglement in the system grows quickly and there is no apparent way to write down local MPOs [41]. In higher dimensions, the tensor contraction is a #P-complete problem [42], rendering most of the traditional tensor-network based methods unfeasible as well.

In this paper, we propose a machine-learning approach for evaluating early-time OTOCs that would bypass these difficulties and work for arbitrary-dimensional systems with massive entanglement. We mention that within physics, applications of machine-learning techniques have recently been boosted in a number of different contexts [43–86], including material design [67], gravitational lenses [64] and wave analysis [65, 66],

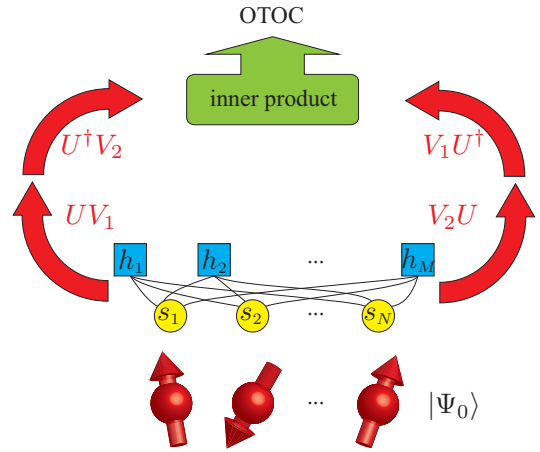


FIG. 1. A pictorial illustration for the computation of out-of-time-ordered correlators (OTOCs) by using restricted Boltzmann machines (RBMs). Considering an arbitrary state  $|\Psi_0\rangle$ , the OTOC as defined in Eq. (1) can be regarded as the overlap between two states  $|\Psi_1\rangle = U^\dagger V_2 U V_1 |\Psi_0\rangle$  and  $|\Psi_2\rangle = V_1 U^\dagger V_2 U |\Psi_0\rangle$  (where  $U = \exp(-iHt)$  is the time-evolution operator), which can be efficiently calculated in the RBM representation.

black hole detection [63], glassy dynamics [68], quantum non-locality detection [85], topological codes [71], quantum machine learning [44, 79], and topological phases and phase transitions [48–57], etc. Here, we focus on one of the simplest stochastic neural networks for unsupervised learning—the restricted Boltzmann machine [87–89] and introduce an RBM-based approach to the numerical computation of OTOCs in quantum many-body systems. Through a concrete example of a 2D transverse field Ising model with system sizes as large as ten-by-ten (which is far beyond the capacity of exact diagonalization), we demonstrate that the proposed RBM-based approach is capable of computing the early-time OTOCs with respect to random pure quantum states or infinite-temperature thermal ensembles. Our method works for generic systems, independent of dimensionality, the amount of entanglement involved, or whether the calculation is performed for regions far away from or near the quantum phase transition point. Our

results showcase the unparalleled power of machine learning in the studies of OTOCs for quantum many-body systems, which paves a novel way to study numerous physical phenomena related to the properties of OTOCs.

*The RBM approach.*—To begin with, let us first briefly introduce the definition of OTOC and the RBM representation of quantum many-body states. An OTOC of a quantum system with Hamiltonian  $H$  is defined as [90]

$$F(t) = \langle V_2^\dagger(t) V_1^\dagger V_2(t) V_1 \rangle, \quad (1)$$

where  $V_1$  and  $V_2$  are two quantum operators and  $V_2(t) = \exp(iHt)V_2 \exp(-iHt)$  is the time-evolved operator in the Heisenberg picture. The expectation value in the above equation can be evaluated with respect to a certain quantum state  $|\psi\rangle$ , such as the ground state of  $H$  or a state that can be easily prepared in the experiment (e.g. Ref. [16, 28]), or with respect to an ensemble of states, such as a thermal ensemble at temperature  $T$  (e.g. Ref. [2, 3]). From the definition in Eq. (1), the evaluation of the OTOC involves the action of operators on the quantum states, their time evolution, and the overlap between different states. In general, the states and operators of an  $N$ -qubit system are represented by vectors and matrices of dimension  $2^N$ , whose storage and manipulation require a formidably huge amount of computational resources when  $N$  is large. This is the major challenge in the numerical evaluation of OTOCs and many other quantities of quantum many-body systems. Fortunately, in practice the physical states and operators we are interested in typically have certain structures and only occupy a tiny corner of the entire Hilbert space, hence possibly allowing much more efficient representations.

One of such efficient representations is the RBM representation, which has attracted considerable attention recently [43, 45, 46, 51, 85]. In an RBM representation, a system of  $N$  spins can be represented by a set of network parameters  $\{a, b, W\}$ . The (unnormalized) many-body wavefunction is given by

$$\Psi(S) = \sum_{\{h_i\}} \exp \left( \sum_j a_j s_j + \sum_i b_i h_i + \sum_{ij} W_{ij} h_i s_j \right), \quad (2)$$

where  $S = (s_1, \dots, s_N)$  with  $s_j = \pm 1$  represents a spin configuration in the  $\sigma_z$  basis;  $h = (h_1, \dots, h_M)$  with  $h_i = \pm 1$  describes the state of  $M$  hidden spin variables;  $a$  and  $b$  are  $N$ - and  $M$ -dimensional complex vectors, and  $W$  an  $M \times N$  complex matrix. After tracing out the hidden spin variables explicitly, the wavefunction can also be written as  $\Psi(S) = \exp \left( \sum_j a_j s_j \right) \prod_i 2 \cosh \left( b_i + \sum_j W_{ij} s_j \right)$ . We mention that any quantum state can be approximated to arbitrary accuracy by the above RBM representation, as long as the number of hidden neurons is large enough [91–93].

Now we introduce the general recipe for computing OTOCs by using the RBM representation. The basic procedure is illustrated schematically in Fig. 1. Suppose the expectation

value in Eq. (1) is with respect to a quantum state  $|\Psi_0\rangle$  represented by an RBM. First, we rewrite the OTOC as the overlap between two states  $|\Psi_1\rangle = V_2(t)V_1|\Psi_0\rangle$  and  $|\Psi_2\rangle = V_1V_2(t)|\Psi_0\rangle$ . Then, we plug in the expression for  $V_2(t)$  and get  $|\Psi_1\rangle = U^\dagger V_2 U V_1 |\Psi_0\rangle$  and  $|\Psi_2\rangle = V_1 U^\dagger V_2 U |\Psi_0\rangle$  where  $U = \exp(-iHt)$  is the time-evolution operator for time  $t$ . Physically it means that the state  $|\Psi_1\rangle$  comes from the initial state  $|\Psi_0\rangle$ , acted on by an operator  $V_1$ , time-evolved for a time interval of  $t$ , further acted on by an operator  $V_2$ , and finally time-evolved backwards for a time interval of  $t$ ; and similar interpretation can be given for the state  $|\Psi_2\rangle$ . Therefore, in order to compute the OTOC, it is of crucial importance that we should be able to find efficient RBM representation of the initial state, to describe the action of operators  $V_1$  and  $V_2$  on an RBM state, to solve the time-evolution of an RBM state, and finally to compute the overlap between two RBM states.

In the definition of OTOC,  $V_1$  and  $V_2$  can be arbitrary operators. Here, we focus on local Pauli operators, which is a natural choice for spin systems and has been widely used in the studies of quantum chaos and information scrambling [3, 8, 9, 12]. Let us consider how the operator  $\sigma_\alpha^k$  ( $\alpha = x, y, z$  and  $k = 1, 2, \dots, N$ ) acts on an RBM state described by the parameters  $\{a, b, W\}$ . The effect of  $\sigma_x^k$  is to flip the  $k$ -th spin. In other words, we want to replace  $s_k$  in Eq. (2) by  $-s_k$  while keeping the value of the wave function unchanged. This can be achieved by updating the RBM parameters  $a_k \rightarrow -a_k$  and  $W_{ik} \rightarrow -W_{ik}$  ( $i = 1, \dots, M$ ). Therefore, to get the new state after the application of  $\sigma_x^k$ , we only need to update  $(M + 1)$  parameters instead of dealing with the  $2^N$ -dimensional state vectors. Next we consider  $\sigma_z^k$ . Its action on an RBM state will not change the spin configuration in the  $\sigma_z$  basis, but introduce a relative phase of  $\pi$  between the  $s_k = \pm 1$  states. Therefore, we can efficiently describe the resulted state after applying  $\sigma_z^k$  by updating  $a_k \rightarrow a_k + i\pi/2$ . Note that in this way we get a global phase factor  $i$  in addition to the desired effect of applying  $\sigma_z^k$  operator. This additional phase factor must be carefully treated when computing the overlap between general states. However, in our calculation of OTOCs, the same operator appears in both  $|\Psi_1\rangle$  and  $|\Psi_2\rangle$  and therefore the phase factors cancel with each other in the inner product. Based on this, we can further implement the  $\sigma_y^k$  operator by consecutive actions of  $\sigma_x^k$  and  $\sigma_z^k$ , without worrying about the global phase factor.

The time evolution of an RBM state can be performed in a similar way as training the ground state [45]. At each step, we try to maximize the fidelity between a new RBM state  $|\Psi(t + \delta t)\rangle$  and the time-evolved state  $(I - iH\delta t)|\Psi(t)\rangle$ . For simplicity in notation here we assume that the states are normalized. Actually, according to Ref. [45], this optimization can be realized by simply using an imaginary learning rate in the algorithm for the ground state. However, in this way we may get an additional phase factor  $|\Psi(t + \delta t)\rangle = e^{i\delta\phi}(I - iH\delta t)|\Psi(t)\rangle$ . Such a global phase is irrelevant in evaluating expectation values since the same phase and its complex conjugate will cancel each other; but for OTOC, we need to compute the overlap between two quantum states,

hence we must keep track of all the phase changes during the evolution. Specifically, we compute the overlap between the states before and after the evolution at each step and get  $\langle \Psi(t) | \Psi(t + \delta t) \rangle = e^{i\delta\phi} (1 - i\bar{E}(t)\delta t)$  where  $\bar{E}(t)$  is the average energy at time  $t$ . In this way we can get the phase shift at each step and then remove them from the final OTOC calculation.

Finally, we consider the overlap between two RBM states  $\langle \Psi_2 | \Psi_1 \rangle / \sqrt{\langle \Psi_1 | \Psi_1 \rangle \langle \Psi_2 | \Psi_2 \rangle}$ , which can be obtained by Monte Carlo sampling of the spin configurations. Specifically, we can sample the spin configuration  $S$  for  $|\Psi_1\rangle$  with relative probability  $|\langle S | \Psi_1 \rangle|^2$ , or normalized probability  $\langle \Psi_1 | S \rangle \langle S | \Psi_1 \rangle / \langle \Psi_1 | \Psi_1 \rangle$ . For each sampled spin configuration, we compute  $\langle S | \Psi_2 \rangle / \langle S | \Psi_1 \rangle$ . By averaging over all the spin configurations, we get  $v_1 = \sum_S \langle \Psi_1 | S \rangle \langle S | \Psi_2 \rangle / \langle \Psi_1 | \Psi_1 \rangle = \langle \Psi_1 | \Psi_2 \rangle / \langle \Psi_1 | \Psi_1 \rangle$ . Similarly we can sample for  $|\Psi_2\rangle$  and compute  $\langle S | \Psi_1 \rangle / \langle S | \Psi_2 \rangle$ . The average value we get is  $v_2 = \langle \Psi_2 | \Psi_1 \rangle / \langle \Psi_2 | \Psi_2 \rangle$ . Combining the two results together we get  $\langle \Psi_2 | \Psi_1 \rangle / \sqrt{\langle \Psi_1 | \Psi_1 \rangle \langle \Psi_2 | \Psi_2 \rangle} = \sqrt{v_1^* v_2}$ .

We stress the difference between our RBM and the conventional TEBD or MPO (or more general tensor-network based) approaches to computing OTOCs. Generally speaking, the TEBD approach relies vitally on the efficient matrix-product-state representation of a quantum many-body state, hence is limited to 1D systems with short-range interactions and small entanglement [41]. The MPO approach exploits the fact that the operators (in the Heisenberg picture) expand at most ballistically for local Hamiltonians with speed bounded by the Lieb-Robinson speed [40], thus is applicable to a much wider space time region than the TEBD approach. Yet, for systems in higher dimensions (larger than one) or with long-range interactions, the MPO approach suffers still since tensor contraction is inefficient in higher dimensions and there is no apparent way to write down local MPOs for systems with long-range interactions. In stark contrast, our RBM approach escapes these limitations owing to the particular neural network structures. It works for higher dimensions and long-range interactions. In addition, since entanglement is not a limiting factor for the efficiency of the RBM representation [46], we expect that it can be used to computing OTOCs for quantum states with massive (e.g., volume-law) entanglement as well. To show more precisely how this RBM approach works, we give a concrete example involving computing OTOCs for a 2D transverse field Ising model, which is beyond the capacity of the TEBD or MPO methods for large system sizes.

*A 2D example.*—We consider a 2D transverse field Ising model on an  $N = L_1 \times L_2$  square lattice with periodic boundary conditions. The Hamiltonian of the system is given by:

$$H = -h \sum_i \sigma_x^i - J \sum_{\langle i, j \rangle} \sigma_z^i \sigma_z^j, \quad (3)$$

where  $\langle i, j \rangle$  denotes all the nearest neighbor spin pairs. This Hamiltonian is rotated by  $90^\circ$  from the commonly used convention [94], with  $\sigma_x$  and  $\sigma_z$  exchanged for convenience. This

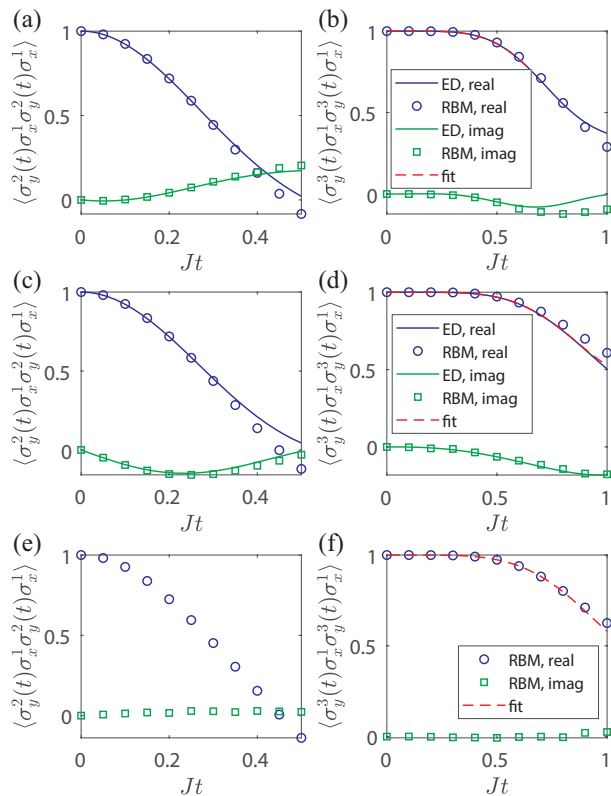


FIG. 2. Comparison between restricted Boltzmann machine (RBM) and exact diagonalization (ED) results for  $N = 3 \times 4$  (first row),  $N = 4 \times 5$  (second row) and  $N = 10 \times 10$  (third row) spins in a transverse field Ising model at  $h/J = 1$ . Here we choose  $V_1 = \sigma_x$  and  $V_2 = \sigma_y$  on the nearest neighbor (first column) and second nearest neighbor (second column) sites. As we can see, both the real and imaginary parts of the RBM result agree well with ED in the early time, and starts to deviate when the OTOC is significantly away from the initial value of one. For the second nearest neighbor case, we fit the early time behavior according to Eq. (4) and consistently obtain  $\lambda \approx 1.9$ ,  $v_f \approx 2.0$  and  $p \approx 0.44$  for different system sizes.

model is one of the simplest toy models for studying quantum phase transitions, despite the fact that it has the same complexity as a 3D classical Ising model whose exact solution still remains a major open question in statistical physics [95]. At zero temperature, a quantum phase transition occurs at  $h/J \approx 3$  according to previous studies [94].

Here, we compute the OTOCs for the above 2D Ising model by using our introduced RBM approach. First we consider random initial RBM states with  $\{a, b, W\}$  following a normal distribution  $N(0, \sigma^2)$  for their real and imaginary parts. For small system sizes we use  $\sigma = 0.1$  while later for a larger system we reduce it to  $\sigma = 0.02$  so as to get better performance for the training of RBM [96]. In Fig. 2(a-d), we show the OTOC results for two system sizes  $N = 3 \times 4$  and  $N = 4 \times 5$  at  $h/J = 1$ , which is away from the phase transition point  $h/J \approx 3$ . From this figure, it is clear that our RBM results match excellently with these from exact diagonalization for small  $Jt$  and deviations become noticeable only after the

OTOCs are significantly away from their initial value. This validates the effectiveness of the RBM approach in computing early-time OTOCs. More strikingly, since the complexity of the RBM approach only scales cubically with increasing  $N$ , we can use it to compute OTOCs for much larger systems. In Fig. 2(e, f), we show part of our OTOC results for a system as large as ten by ten, which is far beyond the capacity of exact diagonalization.

In Ref. [40], Xu and Swingle have conjectured a universal form for the early-time dynamics of OTOCs:

$$\text{Re}[F(t)] \sim 1 - \frac{1}{2} \exp\left(-\lambda \frac{(d - v_f t)^{1+p}}{t^p}\right), \quad (4)$$

where  $v_f$  is the speed of the wavefront and  $d$  is the distance between  $V_1$  and  $V_2$ ; the index  $p$  characterizes the spreading of the wavefront, with  $p = 0$  corresponding to pure exponential decay of  $\text{Re}[F(t)]$  (for holographic models, coupling Sachdev-Ye-Kitaev clusters, etc.),  $p = 1/2$  for non-interacting particle models, and  $p = 1$  for the local random circuit models. Here, we test this conjecture with our RBM results. In Fig. 2, we fit the early time ( $\text{Re}[F(t)] > 0.85$ ) results for all the three system sizes at the distance  $d = 2$  and consistently get  $\lambda \approx 1.9$ ,  $v_f \approx 2.0$  and  $p \approx 0.44$ . This corresponds to a sub-diffusively spreading wavefront [40].

When using RBM-based reinforcement learning to compute the ground state of a Hamiltonian, an observation is that the relative error is usually larger near the critical point due to the divergence of correlation length at the phase transition point [45]. Similar results have also been observed in our calculation of OTOCs. If we take  $|\Psi_0\rangle$  to be a random initial state as in Fig. 2, the relative error of OTOCs computed near the phase transition point is larger than that computed deep in the ferromagnetic/paramagnetic phases. However, if we take  $|\Psi_0\rangle$  to be the ground state of the Hamiltonian (e.g. Ref. [16]), we can still observe excellent agreement between RBM and ED methods even at the transition point, as shown in Fig. 3 for  $N = 4 \times 5$  spins at  $h/J = 3.05$ . In addition, we mention that the accuracy of the OTOCs computed via our RBM method can be systematically improved by increasing the number of hidden neurons or iterations in the training process [45].

In all the above calculations, we compute OTOCs for pure RBM states. In many theoretical works, the OTOC is evaluated with respect to a thermal distribution at inverse temperature  $\beta$ . The  $\beta = 0$  limit corresponds to a uniformly random distribution over all possible spin configurations in our spin model. Since the OTOC is the inner product of two states and thus its absolute value bounded by one, we only need to generate  $s$  random spin configurations to upper-bound the accuracy of the average OTOC to  $1/\sqrt{s}$ . Actually in many cases we are only interested in the real part of OTOC, which is related to the squared out-of-time-ordered commutators [90]. From the previous results we see that it always falls from one and the early-time behavior seems not sensitive to the random choice of initial states; thus we expect the convergence to be much faster. In Fig. 4 we show the infinite temperature OTOC for

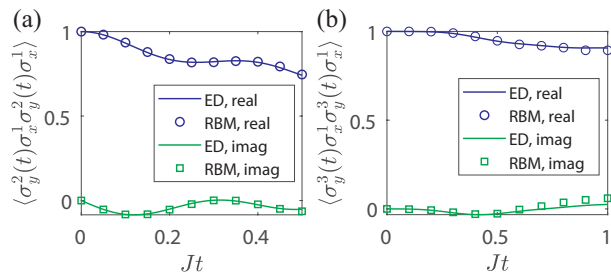


FIG. 3. Comparison between restricted Boltzmann machine (RBM) and exact diagonalization (ED) results for  $N = 4 \times 5$  spins at  $h/J = 3.05$  near the phase transition point of the 2D transverse field Ising model. Again we choose  $V_1 = \sigma_x$  and  $V_2 = \sigma_y$  on the (a) nearest neighbor and (b) second nearest neighbor sites. The initial state  $|\Psi_0\rangle$  is an RBM state trained to the ground state of  $H$ .

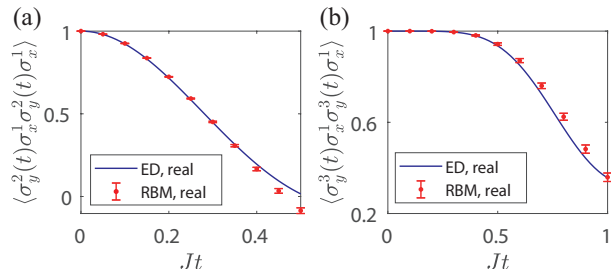


FIG. 4. Comparison between restricted Boltzmann machine (RBM) and exact diagonalization (ED) results for  $N = 3 \times 4$  spins at  $h/J = 1$  and inverse temperature  $\beta = 0$ . Again we consider  $V_1 = \sigma_x$  and  $V_2 = \sigma_y$  on the (a) nearest neighbor and (b) second nearest neighbor sites. The RBM results are averaged over  $s = 10$  randomly generated spin configurations in the  $\sigma_x$  basis. The error bars are estimated from the standard deviation of the average values.

$N = 3 \times 4$  and  $h/J = 1$  by averaging over  $s = 10$  random spin configurations in the  $\sigma_x$  basis, which we generate by training the ground state of Hamiltonian  $H = \sum_i \pm \sigma_x^i$ . The error bars are estimated from the standard deviation of the average values. As we can see, the small number of random realizations  $s = 10$  already leads to good convergence; and the discrepancy between the RBM method and the exact results is mainly caused by the representability of RBM states at large time, similar to the previous examples. Note that in practice the performance of the RBM method is weakened if the initial state is exactly a product state. Thus we choose to train the initial states close to the desired states with small randomness, rather than write down an exact solution.

*Discussion and conclusion.*—Although we only focus our discussion on RBMs in this paper, one may also use other type of neural networks (e.g., deep Boltzmann machine [72] or feedforward neural networks [76], etc.) with different learning algorithms to compute OTOCs for different quantum many-body systems. In particular, it has been proved that deep Boltzmann machine can efficiently represent most physical states, including the ground states of many-body Hamiltonians and states generated by quantum dynamics [72].

Therefore, it would be interesting and important to develop a method based on deep Boltzmann machine to compute OTOCs. A complete study on computing OTOCs with different neural networks would not only bring new powerful tools for solving intricate problems in the quantum many-body physics, but also provide valuable insight in understanding the internal structures of the networks themselves. Moreover, with these new machine learning tools, it would also be interesting and crucial to study certain new physics related to OTOCs, such as information scrambling and dynamical quantum phase transitions in higher dimensions. We leave these interesting topics for future investigation.

To summarize, in this work we describe a general method of computing OTOC in spin systems using RBM ansatz and then present applications in a 2D transverse field Ising model where numerical calculation was challenging with the existing methods. From our numerical examples, it can be seen that the RBM method is suitable for the early-time properties of OTOC such as the Lyapunov exponent [21] and butterfly velocity [3, 23]. The RBM method is not subjected to the limitation of entanglement and geometry, like the conventional method based on local tensor networks, and there is no clear sign problem like the quantum Monte Carlo method. Therefore the RBM method may demonstrate advantages in many models where the other methods are not applicable. On the other hand, what is the limiting factor in the performance of the RBM method is still not clear and can be the topic of future studies.

We thank Jinwu Ye and Shenglong Xu for helpful discussions. This work was supported by the Frontier Science Center for Quantum Information of the Ministry of Education of China, Tsinghua University Initiative Scientific Research Program, and the National key Research and Development Program of China (2016YFA0301902). Y.-K. W. acknowledges support from Shuimu Tsinghua Scholar Program and International Postdoctoral Exchange Fellowship Program (Talent-Introduction Program).

---

\* [lmduan@tsinghua.edu.cn](mailto:lmduan@tsinghua.edu.cn)

† [dldeng@tsinghua.edu.cn](mailto:dldeng@tsinghua.edu.cn)

- [1] A. Larkin and Y. N. Ovchinnikov, “Quasiclassical method in the theory of superconductivity,” *Sov Phys JETP* **28**, 1200 (1969).
- [2] P. Hosur, X.-L. Qi, D. A. Roberts, and B. Yoshida, “Chaos in quantum channels,” *Journal of High Energy Physics* **2016**, 4 (2016).
- [3] M. Mezei and D. Stanford, “On entanglement spreading in chaotic systems,” *Journal of High Energy Physics* **2017**, 65 (2017).
- [4] C. W. von Keyserlingk, T. Rakovszky, F. Pollmann, and S. L. Sondhi, “Operator hydrodynamics, otocs, and entanglement growth in systems without conservation laws,” *Phys. Rev. X* **8**, 021013 (2018).
- [5] A. Nahum, S. Vijay, and J. Haah, “Operator spreading in random unitary circuits,” *Phys. Rev. X* **8**, 021014 (2018).
- [6] D. A. Roberts and B. Swingle, “Lieb-robinson bound and the butterfly effect in quantum field theories,” *Phys. Rev. Lett.* **117**, 091602 (2016).
- [7] A. Bohrdt, C. B. Mendl, M. Endres, and M. Knap, “Scrambling and thermalization in a diffusive quantum many-body system,” *New Journal of Physics* **19**, 063001 (2017).
- [8] Y. Huang, Y.-L. Zhang, and X. Chen, “Out-of-time-ordered correlators in many-body localized systems,” *Annalen der Physik* **529**, 1600318 (2017).
- [9] B. Swingle and D. Chowdhury, “Slow scrambling in disordered quantum systems,” *Phys. Rev. B* **95**, 060201 (2017).
- [10] Y. Chen, “Universal logarithmic scrambling in many body localization,” (2016), [arXiv:1608.02765](https://arxiv.org/abs/1608.02765).
- [11] K. Slagle, Z. Bi, Y.-Z. You, and C. Xu, “Out-of-time-order correlation in marginal many-body localized systems,” *Phys. Rev. B* **95**, 165136 (2017).
- [12] C. B. Dağ and L.-M. Duan, “Detection of out-of-time-order correlators and information scrambling in cold atoms: Ladder-XX model,” *Phys. Rev. A* **99**, 052322 (2019).
- [13] D. A. Roberts and D. Stanford, “Diagnosing chaos using four-point functions in two-dimensional conformal field theory,” *Phys. Rev. Lett.* **115**, 131603 (2015).
- [14] J. Maldacena, S. H. Shenker, and D. Stanford, “A bound on chaos,” *Journal of High Energy Physics* **2016**, 106 (2016).
- [15] I. Kukuljan, S. c. v. Grozdanov, and T. c. v. Prosen, “Weak quantum chaos,” *Phys. Rev. B* **96**, 060301 (2017).
- [16] M. Heyl, F. Pollmann, and B. Dóra, “Detecting equilibrium and dynamical quantum phase transitions in ising chains via out-of-time-ordered correlators,” *Phys. Rev. Lett.* **121**, 016801 (2018).
- [17] R. Fan, P. Zhang, H. Shen, and H. Zhai, “Out-of-time-order correlation for many-body localization,” *Science Bulletin* **62**, 707 (2017).
- [18] C. B. Dağ, K. Sun, and L.-M. Duan, “Detection of quantum phases via out-of-time-order correlators,” *Phys. Rev. Lett.* **123**, 140602 (2019).
- [19] J. Maldacena, “The large-n limit of superconformal field theories and supergravity,” *International Journal of Theoretical Physics* **38**, 1113 (1999).
- [20] Y. Sekino and L. Susskind, “Fast scramblers,” *Journal of High Energy Physics* **2008**, 065 (2008).
- [21] S. H. Shenker and D. Stanford, “Black holes and the butterfly effect,” *Journal of High Energy Physics* **2014**, 67 (2014).
- [22] S. H. Shenker and D. Stanford, “Multiple shocks,” *Journal of High Energy Physics* **2014**, 46 (2014).
- [23] D. A. Roberts, D. Stanford, and L. Susskind, “Localized shocks,” *Journal of High Energy Physics* **2015**, 51 (2015).
- [24] S. H. Shenker and D. Stanford, “Stringy effects in scrambling,” *Journal of High Energy Physics* **2015**, 132 (2015).
- [25] K. Jensen, “Chaos in  $ads_2$  holography,” *Phys. Rev. Lett.* **117**, 111601 (2016).
- [26] J. Maldacena, D. Stanford, and Z. Yang, “Diving into traversable wormholes,” *Fortschritte der Physik* **65**, 1700034 (2017).
- [27] B. Yoshida and A. Kitaev, “Efficient decoding for the hayden-preskill protocol,” (2017), [arXiv:1710.03363](https://arxiv.org/abs/1710.03363).
- [28] M. Gärtner, J. G. Bohnet, A. Safavi-Naini, M. L. Wall, J. J. Bollinger, and A. M. Rey, “Measuring out-of-time-order correlations and multiple quantum spectra in a trapped-ion quantum magnet,” *Nature Physics* **13**, 781 (2017).
- [29] J. Li, R. Fan, H. Wang, B. Ye, B. Zeng, H. Zhai, X. Peng, and J. Du, “Measuring out-of-time-order correlators on a nuclear magnetic resonance quantum simulator,” *Phys. Rev. X* **7**, 031011 (2017).
- [30] K. X. Wei, C. Ramanathan, and P. Cappellaro, “Exploring localization in nuclear spin chains,”

- Phys. Rev. Lett.* **120**, 070501 (2018).
- [31] E. J. Meier, J. Ang'ong'a, F. A. An, and B. Gadway, "Exploring quantum signatures of chaos on a floquet synthetic lattice," *Phys. Rev. A* **100**, 013623 (2019).
- [32] R. S. Michalski, J. G. Carbonell, and T. M. Mitchell, *Machine learning: An artificial intelligence approach* (Springer Science & Business Media, 2013).
- [33] Y. LeCun, Y. Bengio, and G. Hinton, "Deep learning," *Nature* **521**, 436 (2015).
- [34] M. Jordan and T. Mitchell, "Machine learning: Trends, perspectives, and prospects," *Science* **349**, 255 (2015).
- [35] A. Kitaev, "A simple model of quantum holography," <http://online.kitp.ucsb.edu/online/entangled15/kitaev/>, <http://online.kitp.ucsb.edu/online/entangled15/kitaev2/> (2015).
- [36] J. Polchinski and V. Rosenhaus, "The spectrum in the sachdev-ye-kitaev model," *Journal of High Energy Physics* **2016**, 1 (2016).
- [37] J. Maldacena and D. Stanford, "Remarks on the sachdev-ye-kitaev model," *Phys. Rev. D* **94**, 106002 (2016).
- [38] M. McGinley, A. Nunnenkamp, and J. Knolle, "Slow growth of out-of-time-order correlators and entanglement entropy in integrable disordered systems," *Phys. Rev. Lett.* **122**, 020603 (2019).
- [39] C.-J. Lin and O. I. Motrunich, "Out-of-time-ordered correlators in a quantum ising chain," *Phys. Rev. B* **97**, 144304 (2018).
- [40] S. Xu and B. Swingle, "Accessing scrambling using matrix product operators," (2018), [arXiv:1802.00801](https://arxiv.org/abs/1802.00801).
- [41] U. Schollwöck, "The density-matrix renormalization group in the age of matrix product states," *Ann. of Phys.* **326**, 96 (2011).
- [42] A. García-Sáez and J. I. Latorre, "An exact tensor network for the 3sat problem," *Quantum Information and Computation* **12**, 0283 (2012).
- [43] G. Carleo, I. Cirac, K. Cranmer, L. Daudet, M. Schuld, N. Tishby, L. Vogt-Maranto, and L. Zdeborová, "Machine learning and the physical sciences," [arXiv:1903.10563](https://arxiv.org/abs/1903.10563) (2019).
- [44] S. D. Sarma, D.-L. Deng, and L.-M. Duan, "Machine learning meets quantum physics," *Physics Today* **72**, 48 (2019).
- [45] G. Carleo and M. Troyer, "Solving the quantum many-body problem with artificial neural networks," *Science* **355**, 602 (2017).
- [46] D.-L. Deng, X. Li, and S. Das Sarma, "Quantum entanglement in neural network states," *Phys. Rev. X* **7**, 021021 (2017).
- [47] L.-F. Arsenault, O. A. von Lilienfeld, and A. J. Millis, "Machine learning for many-body physics: efficient solution of dynamical mean-field theory," [arXiv:1506.08858](https://arxiv.org/abs/1506.08858) (2015).
- [48] Y. Zhang and E.-A. Kim, "Quantum loop topography for machine learning," *Phys. Rev. Lett.* **118**, 216401 (2017).
- [49] J. Carrasquilla and R. G. Melko, "Machine learning phases of matter," *Nat. Phys.* **13**, 431 (2017).
- [50] E. P. van Nieuwenburg, Y.-H. Liu, and S. D. Huber, "Learning phase transitions by confusion," *Nat. Phys.* **13**, 435 (2017).
- [51] D.-L. Deng, X. Li, and S. Das Sarma, "Machine learning topological states," *Phys. Rev. B* **96**, 195145 (2017).
- [52] L. Wang, "Discovering phase transitions with unsupervised learning," *Phys. Rev. B* **94**, 195105 (2016).
- [53] P. Broecker, J. Carrasquilla, R. G. Melko, and S. Trebst, "Machine learning quantum phases of matter beyond the fermion sign problem," *Sci. Rep.* **7** (2017), [10.1038/s41598-017-09098-0](https://doi.org/10.1038/s41598-017-09098-0).
- [54] K. Ch'ng, J. Carrasquilla, R. G. Melko, and E. Khatami, "Machine learning phases of strongly correlated fermions," *Phys. Rev. X* **7**, 031038 (2017).
- [55] Y. Zhang, R. G. Melko, and E.-A. Kim, "Machine learning  $z_2$  quantum spin liquids with quasiparticle statistics," *Phys. Rev. B* **96**, 245119 (2017).
- [56] S. J. Wetzal, "Unsupervised learning of phase transitions: From principal component analysis to variational autoencoders," *Phys. Rev. E* **96**, 022140 (2017).
- [57] W. Hu, R. R. P. Singh, and R. T. Scalettar, "Discovering phases, phase transitions, and crossovers through unsupervised machine learning: A critical examination," *Phys. Rev. E* **95**, 062122 (2017).
- [58] N. Yoshioka, Y. Akagi, and H. Katsura, "Learning disordered topological phases by statistical recovery of symmetry," *Phys. Rev. B* **97**, 205110 (2018).
- [59] G. Torlai and R. G. Melko, "Learning thermodynamics with boltzmann machines," *Phys. Rev. B* **94**, 165134 (2016).
- [60] K.-I. Aoki and T. Kobayashi, "Restricted boltzmann machines for the long range ising models," *Mod. Phys. Lett. B* , 1650401 (2016).
- [61] Y.-Z. You, Z. Yang, and X.-L. Qi, "Machine learning spatial geometry from entanglement features," *Phys. Rev. B* **97**, 045153 (2018).
- [62] G. Torlai, G. Mazzola, J. Carrasquilla, M. Troyer, R. Melko, and G. Carleo, "Neural-network quantum state tomography," *Nat. Phys.* , 1 (2018).
- [63] M. Pasquato, "Detecting intermediate mass black holes in globular clusters with machine learning," [arXiv:1606.08548](https://arxiv.org/abs/1606.08548) (2016).
- [64] Y. D. Hezaveh, L. Perreault Levasseur, and P. J. Marshall, "Fast automated analysis of strong gravitational lenses with convolutional neural networks," *Nature* **548**, 555 (2017).
- [65] R. Biswas, L. Blackburn, J. Cao, R. Essick, K. A. Hodge, E. Katsavounidis, K. Kim, Y.-M. Kim, E.-O. Le Bigot, C.-H. Lee, J. J. Oh, S. H. Oh, E. J. Son, Y. Tao, R. Vaulin, and X. Wang, "Application of machine learning algorithms to the study of noise artifacts in gravitational-wave data," *Phys. Rev. D* **88**, 062003 (2013).
- [66] B. P. Abbott *et al.* (LIGO Scientific Collaboration and Virgo Collaboration), "Observation of gravitational waves from a binary black hole merger," *Phys. Rev. Lett.* **116**, 061102 (2016).
- [67] S. V. Kalinin, B. G. Sumpter, and R. K. Archibald, "Big-deep-smart data in imaging for guiding materials design," *Nat. Mater.* **14**, 973 (2015).
- [68] S. S. Schoenholz, E. D. Cubuk, D. M. Sussman, E. Kaxiras, and A. J. Liu, "A structural approach to relaxation in glassy liquids," *Nat. Phys.* **12**, 469 (2016).
- [69] J. Liu, Y. Qi, Z. Y. Meng, and L. Fu, "Self-learning monte carlo method," *Phys. Rev. B* **95**, 041101 (2017).
- [70] L. Huang and L. Wang, "Accelerated monte carlo simulations with restricted boltzmann machines," *Phys. Rev. B* **95**, 035105 (2017).
- [71] G. Torlai and R. G. Melko, "Neural decoder for topological codes," *Phys. Rev. Lett.* **119**, 030501 (2017).
- [72] X. Gao and L.-M. Duan, "Efficient representation of quantum many-body states with deep neural networks," *Nat. Commu.* , 662 (2017).
- [73] J. Chen, S. Cheng, H. Xie, L. Wang, and T. Xiang, "Equivalence of restricted boltzmann machines and tensor network states," *Phys. Rev. B* **97**, 085104 (2018).
- [74] Y. Huang and J. E. Moore, "Neural network representation of tensor network and chiral states," [arXiv:1701.06246](https://arxiv.org/abs/1701.06246) (2017).
- [75] F. Schindler, N. Regnault, and T. Neupert, "Probing many-body localization with neural networks," *Phys. Rev. B* **95**, 245134 (2017).
- [76] Z. Cai and J. Liu, "Approximating quantum many-body wave functions using artificial neural networks," *Phys. Rev. B* **97**, 035116 (2018).

- [77] P. Broecker, F. F. Assaad, and S. Trebst, “Quantum phase recognition via unsupervised machine learning,” [arXiv:1707.00663](https://arxiv.org/abs/1707.00663) (2017).
- [78] Y. Nomura, A. S. Darmawan, Y. Yamaji, and M. Imada, “Restricted boltzmann machine learning for solving strongly correlated quantum systems,” *Phys. Rev. B* **96**, 205152 (2017).
- [79] J. Biamonte, P. Wittek, N. Pancotti, P. Rebentrost, N. Wiebe, and S. Lloyd, “Quantum machine learning,” *Nature* **549**, 195 (2017).
- [80] S. Lu, S. Huang, K. Li, J. Li, J. Chen, D. Lu, Z. Ji, Y. Shen, D. Zhou, and B. Zeng, “Separability-entanglement classifier via machine learning,” *Phys. Rev. A* **98**, 012315 (2018).
- [81] S. Weinstein, “Learning the einstein-podolsky-rosen correlations on a restricted boltzmann machine,” [arXiv preprint arXiv:1707.03114](https://arxiv.org/abs/1707.03114) (2017).
- [82] H. Saito, “Solving the bose–hubbard model with machine learning,” *J. Phys. Soc. Jpn.* **86**, 093001 (2017).
- [83] H. Saito and M. Kato, “Machine learning technique to find quantum many-body ground states of bosons on a lattice,” *J. Phys. Soc. Jpn.* **87**, 014001 (2017).
- [84] M. Schmitt and M. Heyl, “Quantum dynamics in transverse-field ising models from classical networks,” *SciPost Phys.* **4**, 013 (2018).
- [85] D.-L. Deng, “Machine learning detection of bell nonlocality in quantum many-body systems,” *Phys. Rev. Lett.* **120**, 240402 (2018).
- [86] Y.-T. Hsu, X. Li, D.-L. Deng, and S. Das Sarma, “Machine learning many-body localization: Search for the elusive nonergodic metal,” *Phys. Rev. Lett.* **121**, 245701 (2018).
- [87] G. E. Hinton and R. R. Salakhutdinov, “Reducing the dimensionality of data with neural networks,” *Science* **313**, 504 (2006).
- [88] R. Salakhutdinov, A. Mnih, and G. Hinton, “Restricted boltzmann machines for collaborative filtering,” in *Proceedings of the 24th international conference on Machine learning* (ACM, 2007) pp. 791–798.
- [89] H. Larochelle and Y. Bengio, “Classification using discriminative restricted boltzmann machines,” in *Proceedings of the 25th international conference on Machine learning* (ACM, 2008) pp. 536–543.
- [90] B. Swingle, “Unscrambling the physics of out-of-time-order correlators,” *Nature Physics* **14**, 988 (2018).
- [91] A. N. Kolmogorov, “On the representation of continuous functions of many variables by superposition of continuous functions of one variable and addition,” *Amer. Math. Soc. Transl* **28**, 55 (1963).
- [92] N. Le Roux and Y. Bengio, “Representational power of restricted boltzmann machines and deep belief networks,” *Neural Comput.* **20**, 1631 (2008).
- [93] K. Hornik, “Approximation capabilities of multilayer feedforward networks,” *Neural networks* **4**, 251 (1991).
- [94] A. Montakhab and A. Asadian, “Multipartite entanglement and quantum phase transitions in the one-, two-, and three-dimensional transverse-field ising model,” *Phys. Rev. A* **82**, 062313 (2010).
- [95] B. K. Chakrabarti, A. Dutta, and P. Sen, *Quantum Ising phases and transitions in transverse Ising models*, Vol. 41 (Springer Science & Business Media, 2008).
- [96] G. E. Hinton, “A practical guide to training restricted boltzmann machines,” in *Neural Networks: Tricks of the Trade: Second Edition*, edited by G. Montavon, G. B. Orr, and K.-R. Müller (Springer Berlin Heidelberg, Berlin, Heidelberg, 2012) pp. 599–619.